Acta Cryst E CRYSTALLOGRAPHIC COMMUNICATIONS

ISSN 2056-9890

1-Chloro-4-[2-(4-chlorophenyl)ethyl]benzene and its bromo analogue: crystal structure, Hirshfeld surface analysis and computational chemistry

Mukesh M. Jotani,[a]‡ See Mun Lee,[b] Kong Mun Lo[b] and Edward R. T. Tiekink[b]*

[a]Department of Physics, Bhavan's Sheth R. A. College of Science, Ahmedabad, Gujarat 380001, India, and [b]Research Centre for Crystalline Materials, School of Science and Technology, Sunway University, 47500 Bandar Sunway, Selangor Darul Ehsan, Malaysia. *Correspondence e-mail: edwardt@sunway.edu.my

Received 2 April 2019
Accepted 8 April 2019

Edited by W. T. A. Harrison, University of Aberdeen, Scotland

‡ Additional correspondence author, e-mail: mmjotani@rediffmail.com.

Keywords: crystal structure; 1,2-bis(phenyl)ethane; Hirshfeld surface analysis; interaction energies.

CCDC references: 1908484; 1908483

Supporting information: this article has supporting information at journals.iucr.org/e

The crystal and molecular structures of $C_{14}H_{12}Cl_2$, (I), and $C_{14}H_{12}Br_2$, (II), are described. The asymmetric unit of (I) comprises two independent molecules, *A* and *B*, each disposed about a centre of inversion. Each molecule approximates mirror symmetry [the $C_b-C_b-C_e-C_e$ torsion angles = −83.46 (19) and 95.17 (17)° for *A*, and −83.7 (2) and 94.75 (19)° for *B*; b = benzene and e = ethylene]. By contrast, the molecule in (II) is twisted, as seen in the dihedral angle of 59.29 (11)° between the benzene rings *cf.* 0° in (I). The molecular packing of (I) features benzene-C—H···π(benzene) and Cl···Cl contacts that lead to an open three-dimensional (3D) architecture that enables twofold 3D–3D interpenetration. The presence of benzene-C—H···π(benzene) and Br···Br contacts in the crystal of (II) consolidate the 3D architecture. The analysis of the calculated Hirshfeld surfaces confirm the influence of the benzene-C—H···π(benzene) and *X*···*X* contacts on the molecular packing and show that, to a first approximation, H···H, C···H/H···C and C···*X*/*X*···C contacts dominate the packing, each contributing about 30% to the overall surface in each of (I) and (II). The analysis also clearly differentiates between the *A* and *B* molecules of (I).

1. Chemical context

The synthesis and physical characterization of the title compound, 1-chloro-4-[2-(4-chlorophenyl)ethyl]benzene, $C_{14}H_{12}Cl_2$, (I), has been reported by several research groups over the years (Otsubo *et al.*, 1980; Bestiuc *et al.*, 1985; Parnes *et al.*, 1989; Hu *et al.*, 2011; Liu & Li, 2007). In the same way, the bromo analogue of (I), 1-bromo-4-[2-(4-bromophenyl)ethyl]benzene, $C_{14}H_{12}Br_2$, (II), has been described previously (Golden, 1961; Otsubo *et al.*, 1980; Remizov *et al.*, 2005; Liu & Li, 2007). Despite this interest, crystallographic characterization is lacking. Recently, compounds (I) and (II) became available as minor side-products during the synthesis of the respective tri(4-halobenzyl)tin hydroxide from the reaction of tri(4-halobenzyl)tin halide and sodium hydroxide. Herein, the crystal and molecular structures of (I) and (II) are described. The structures are not isostructural and in order to gain further insight into the molecular packing, the structures were subjected to an analysis of their Hirshfeld surfaces along with some computational chemistry.

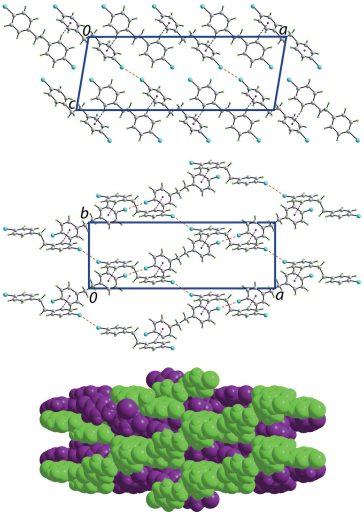

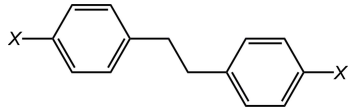

(I) *X* = Cl; (II) *X* = Br

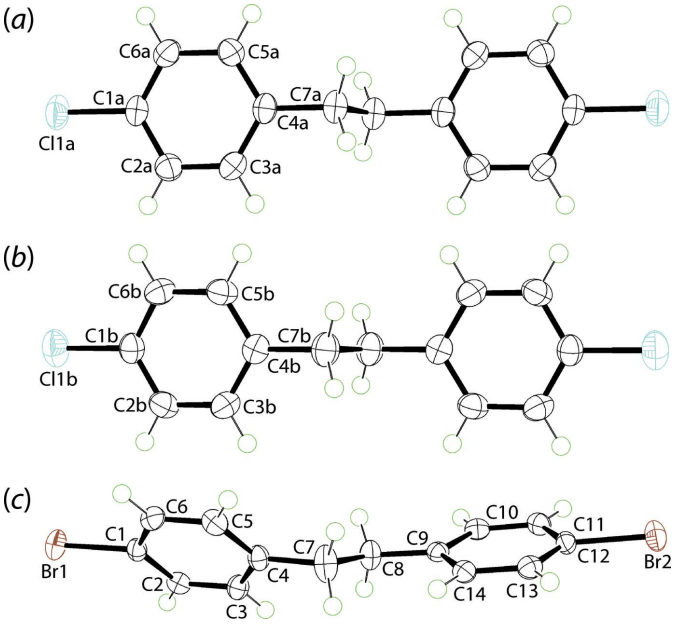

Figure 1
The molecular structures of (*a*) the Cl1*A*-containing molecule of (I), (*b*) the Cl1*B*-containing molecule of (I) and (*c*) the molecule of (II) showing the atom-labelling scheme and displacement ellipsoids at the 70% probability level. Unlabelled atoms in (*a*) and (*b*) are related by the symmetry operations $1-x, 1-y, 1-z$ and $\frac{1}{2}-x, \frac{3}{2}-y, 1-z$, respectively.

2. Structural commentary

The two independent molecules comprising the asymmetric unit of (I) are shown in Fig. 1(*a*) and (*b*); each is disposed about a centre of inversion. The molecules present very similar features and, from inversion symmetry, comprise parallel benzene rings. The C3*A*—C4*A*—C7*A*—C7*A*^{i} and C5*A*—C4*A*—C7*A*—C7*A*^{i} torsion angles of −83.46 (19) and 95.17 (17)° highlight deviations from mirror symmetry in the molecule [symmetry operation: (i) $1-x, 1-y, 1-z$]. These values are equal within experimental error and are very close to the equivalent angles for the second independent molecule of −83.7 (2) and 94.75 (19)°, respectively [symmetry operation: (ii) $\frac{1}{2}-x, \frac{3}{2}-y, 1-z$].

The molecule of (II) is shown in Fig. 1(*c*) and does not feature the molecular symmetry of (I). The difference in the conformation in (II), *cf.* (I), is seen immediately in the magnitude of the dihedral angle formed between the benzene rings of 59.29 (11)°, indicating an inclined disposition. The central torsion angle, *i.e.* C4—C7—C8—C9 of 172.1 (2)°, deviates from the 180° angles observed for the two independent molecules in (I). The twist in the molecule of (II) is reflected in the four torsion angles C3—C4—C7—C8 [46.6 (3)°], C5—C4—C7—C8 [−134.8 (2)°], C7—C8—C9—C14 [16.4 (3)°] and C7—C8—C9—C10 [−163.7 (2)°].

The conformational differences between the molecules in (I) and (II) are highlighted in the overlay diagram shown in Fig. 2.

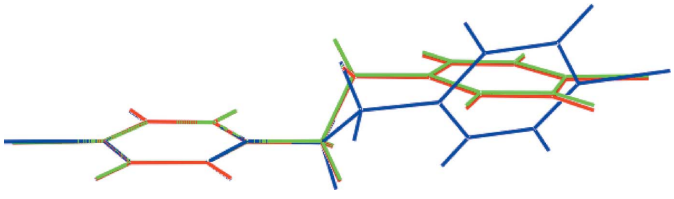

Figure 2
Overlap diagram of the (*a*) Cl1*A*-molecule in (I) (red image), (*b*) Cl1*B*-molecule in (I) (green) and (*c*) the molecule in (II) (blue). Molecules have been overlapped so that the C1-benzene rings are coincident.

Table 1
Hydrogen-bond geometry (Å, °) for (I).

*Cg*1 is the centroid of the (C1*A*–C6*A*) ring.

D—H···*A*	*D*—H	H···*A*	*D*···*A*	*D*—H···*A*
C5*B*—H5*B*···*Cg*1	0.93	2.62	3.4866 (15)	155

3. Supramolecular features

In the crystal of (I), the main point of contact between the independent molecules comprising the asymmetric unit are of the type benzene-C—H···π(benzene), Table 1. The result is

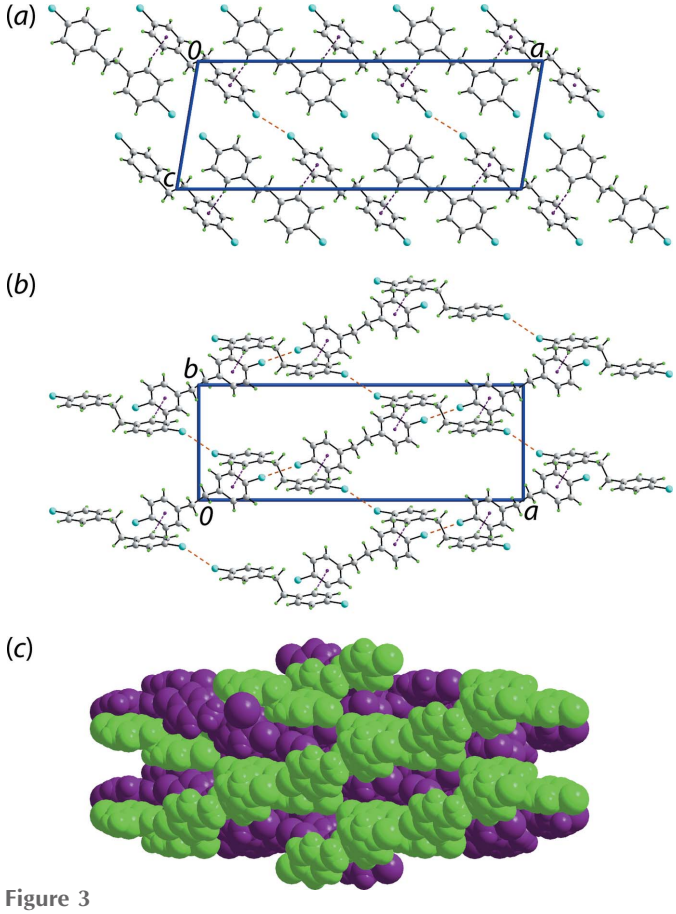

Figure 3
Molecular packing in (I): (*a*) a view of the supramolecular layer parallel to [1$\bar{1}$0] sustained by C—H···π and Cl···Cl contacts shown as purple and orange dashed lines, respectively, (*b*) a view of half of the unit-cell contents shown in projection down the *c* axis and (*c*) an image highlighting the twofold interpenetration in space-filling mode.

Table 2
Hydrogen-bond geometry (Å, °) for (II).

*Cg*1 and *Cg*2 are the centroids of the (C1–C6) and (C9–C14) rings, respectively.

D—H···*A*	*D*—H	H···*A*	*D*···*A*	*D*—H···*A*
C3—H3···*Cg*2^{i}	0.95	2.69	3.442 (2)	136
C6—H6···*Cg*1^{ii}	0.95	2.91	3.704 (2)	141
C13—H13···*Cg*2^{iii}	0.95	2.87	3.569 (2)	131

Symmetry codes: (i) $-x, -y+1, -z+1$; (ii) $-x+1, y+\frac{1}{2}, -z+\frac{3}{2}$; (iii) $-x, y-\frac{1}{2}, -z+\frac{1}{2}$.

the formation of a supramolecular chain along the *a*-axis direction. Chains are connected into a supramolecular layer *via* end-on Cl1*A*···Cl1*A*^{iii} contacts [3.3184 (7) Å and C1—Cl1*A*···Cl1*A*^{iii} = 164.61 (5)° for symmetry operation (iii) $\frac{1}{2}-x, \frac{3}{2}-y, -z$], Fig. 3(*a*). The topology of the layer is flat and connections between the layers that stack along [1$\bar{1}$0] are weaker end-on Cl1*B*···Cl1*B*^{iv} contacts [3.4322 (7) Å and C1*B*—Cl1*B*···Cl1*B*^{iv} = 155.19 (5)° for symmetry operation (iv) $1-x, 2-y, 2-z$], which lead to a three-dimensional (3-D) architecture. As seen from Fig, 3(*b*), there are large voids defined by the aforementioned contacts which enables twofold, 3D–3D interpenetration, Fig. 3(*c*).

The 3-D architecture of (II) is supported by benzene-C—H···π(benzene) and Br···Br contacts. Globally, molecules assemble in the *ac* plane and are connected to layers along [010] by benzene-C—H···π(benzene) contacts, Table 2. Further, lateral interactions are Br1···Br2^{i} [3.5242 (4) Å, C1—Br···Br2^{i} = 144.67 (7)° and C12^{i}—Br2^{i}···Br1 = 154.39 (7)° for symmetry operation (i) $1+x, y, 1+z$; Fig. 4].

4. Hirshfeld surface analysis

The Hirshfeld surface calculations for (I) and (II) were performed in accord with established procedures (Tan *et al.*, 2019) with the aid of *Crystal Explorer* (Turner *et al.*, 2017) to determine the influence of weak intermolecular interactions upon the molecular packing in the absence of conventional hydrogen bonds.

In the crystal of (I), with two independent molecules, labelled *A* and *B*, disposed about a centre of inversion the

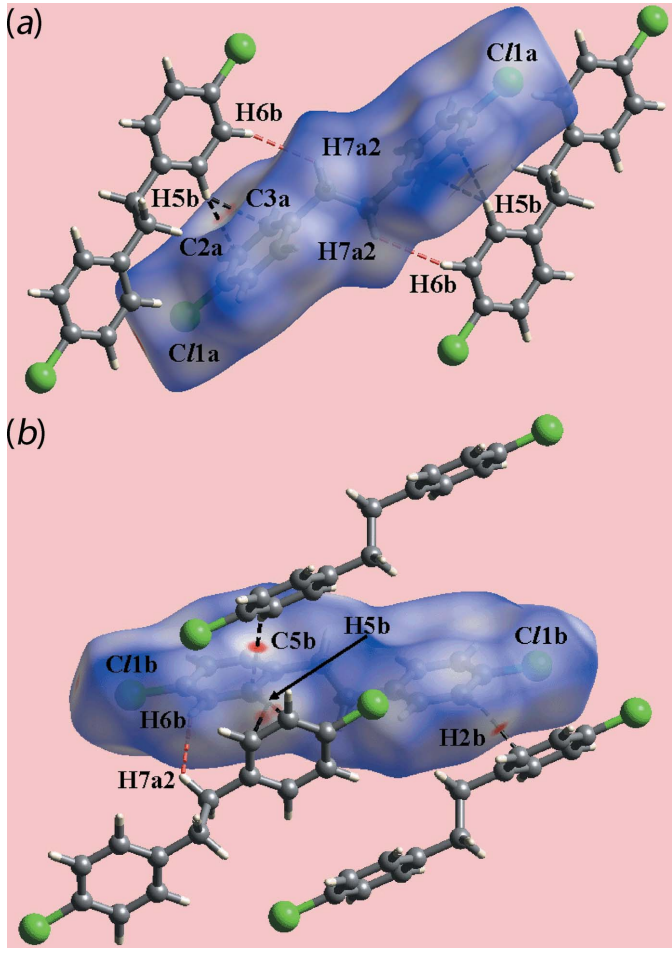

Figure 5
Views of the Hirshfeld surfaces for (I) mapped over d_{norm} for (*a*) molecule *A* [in the range −0.103 to +1.259 arbitrary units] and (*b*) molecule *B* [−0.072 to +1.234 arbitrary units] highlighting the short interatomic C···H/H···C and H···H contacts through black and red dashed lines, respectively.

presence of faint-red spots near the benzene-C2*A*, C3*A* and H5*B* atoms in the images of Hirshfeld surfaces mapped over d_{norm} in Fig. 5 represent C—H···π contacts, Tables 1 and 3. The diminutive red spot viewed near the benzene-C5*B* atom in Fig. 5(*b*) indicates the effect of a short interatomic C5*B*···H2*B*

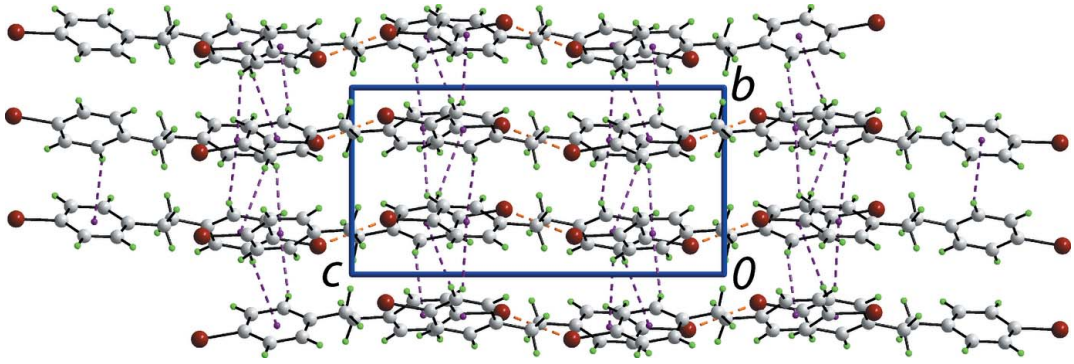

Figure 4
Molecular packing in (II): a view of the unit-cell contents shown in projection down the *a* axis, highlighting C—H···π and Br···Br contacts as purple and orange dashed lines, respectively.

Table 3
Summary of short interatomic contacts (Å) in (I)[a].

Contact	Distance	Symmetry operation
(I)		
H6*B*···H72*A*	2.35	x, y, z
H5*B*···C2*A*	2.75	x, y, z
H5*B*···C3*A*	2.72	x, y, z
H2*B*···C5*B*	2.67	$x, 2-y, \frac{1}{2}+z$
C11*A*···Cl1*A*	3.3184 (7)	$\frac{1}{2}-x, \frac{3}{2}-y, -z$
Cl1*B*···Cl1*B*	3.4322 (7)	$1-x, 2-y, 2-z$
(II)		
H8*B*···H8*B*	2.21	$-x, 2-y, 1-z$
H3···C13	2.74	$-x, 1-y, 1-z$
H3···C14	2.72	$-x, 1-y, 1-z$
H6···C1	2.82	$1-x, \frac{1}{2}+y, \frac{3}{2}-z$
H6···C2	2.62	$1-x, \frac{1}{2}+y, \frac{3}{2}-z$
H11···C6	2.80	$-x, 2-y, 1-z$
Br1···Br2	3.5242 (4)	$1+x, y, 1+z$

Notes: (*a*) The interatomic distances are calculated in *Crystal Explorer* (Turner *et al.*, 2017) whereby the *X*—H bond lengths are adjusted to their neutron values.

contact, Table 3. Also, the presence of diminutive red spots near the terminal chlorine atoms of both independent molecules in Fig. 5 are due to the formation of short interatomic Cl···Cl contacts, Table 3.

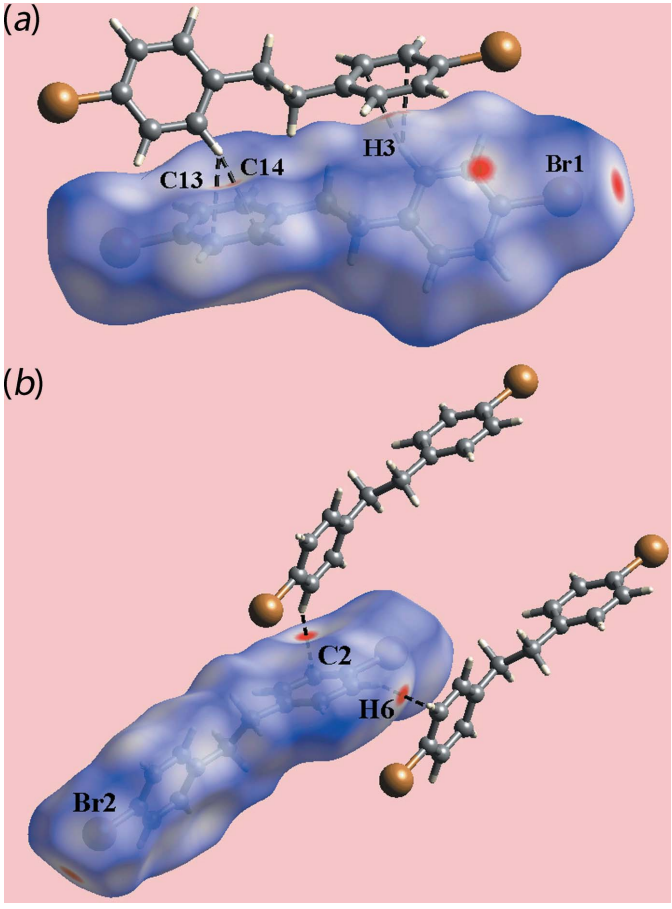

Figure 6
Views of the Hirshfeld surfaces for (II) mapped over d_{norm} [in the range −0.104 to +1.172 arbitrary units] highlighting the short interatomic C···H/H···C contacts through black dashed lines.

In the crystal of (II), the bright-red spots near the bromine atoms on the Hirshfeld surfaces mapped over d_{norm} in Fig. 6 indicate interatomic Br···Br contacts, Table 3, whereas those near the benzene-C2 and H6 atoms in Fig. 6(*b*) indicate short interatomic C—H···π interactions, Table 3. The presence of faint-red spots near the benzene-C13, C14 and H3 atoms in Fig. 6(*a*) also reflect the presence of C—H···π contacts, Table 3.

From the views of Hirshfeld surfaces mapped over the calculated electrostatic potentials in Figs. 7(*a*) and (*b*) for the independent molecules of (I) highlight the small deviations from putative mirror symmetry through the slight differences in the blue and red regions around the atoms of their surfaces corresponding, respectively, to positive and negative potentials. For (II), Fig.7(*c*), the donors and acceptors of the C—H···π interactions are viewed as blue bumps and light-red concave regions. Further, the donors and acceptors of the C—H···π contacts for each of (I) and (II) are also illustrated through black dotted lines on the Hirshfeld surfaces mapped with shape-index properties in Fig. 8.

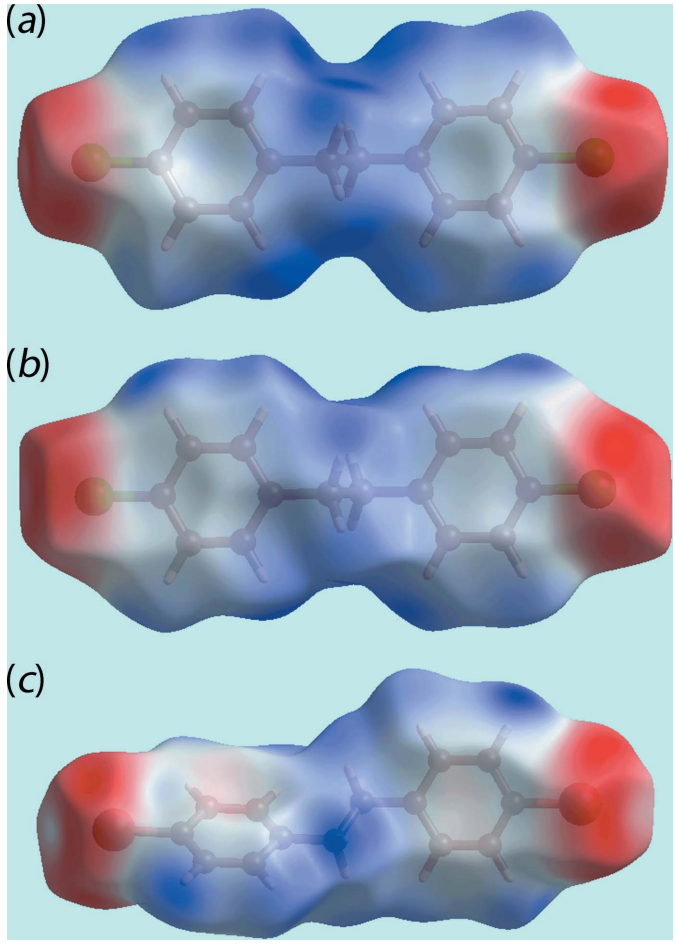

Figure 7
Views of the Hirshfeld surfaces mapped over the calculated electrostatic potential for (*a*) (I), molecule *A* [−0.032 to +0.035 a.u.], (*b*) (I), molecule *B* in [−0.033 to +0.044 a.u.] range and (*c*) (II) [−0.022 to +0.039 a.u.]. The red and blue regions represent negative and positive electrostatic potentials, respectively.

Table 4
Percentage contributions of interatomic contacts to the Hirshfeld surface for (I) and (II).

Contact	Percentage contribution			
	(I) - molecule *A*	(I) - molecule *B*	(I)	(II)
H···H	30.8	35.1	31.4	30.6
C···H/H···C	32.5	27.0	28.4	32.7
X···H/H···*X*	30.5	33.3	34.2	30.4
X···*X*	3.9	2.2	3.4	4.9
C···C	1.3	1.3	1.4	0.0
C···*X*/*X*···C	1.1	1.1	1.2	1.4

The overall two-dimensional fingerprint plot for the independent molecules *A* and *B* as well as entire (I) are shown in Fig. 9(*a*), and those delineated into H···H, C···H/H···C, Cl···H/H···Cl and Cl···Cl contacts are illustrated in Fig. 9(*b*)–(*e*), respectively. The quantitative summary of percentage contributions from the different interatomic contacts to the respective Hirshfeld surfaces of *A*, *B* and (I) are presented in Table 4.

Some qualitative differences in the fingerprint plots are evident for molecules *A* and *B*, confirming their distinct packing interactions. The complementary pair of forceps-like tips at $d_e + d_i$ ~2.3 Å in the fingerprint plots delineated into H···H contacts for *A* and *B* in Fig. 9(*b*) represent the short interatomic H···H contact, Table 3, which merge to form a pair of tips in the overall plot for (I). The fingerprint plots delineated into C···H/H···C contacts for molecules *A* and *B* in Fig. 9(*c*) exhibit the clearest distinction between the interatomic contacts formed by the molecules through the asymmetric distribution of points. The complementary distribution of points in the acceptor and donor regions of the plots for *A* and *B*, respectively, with the peaks at $d_e + d_i$ ~2.7 Å, are due to the formation of short interatomic C···H/H···C contacts between the benzene-C2*A*, C3*A* and H5*B* atoms, Table 3. Similar short interatomic contacts between benzene-C5*B* and H2*B* atoms of *B* results in forceps-like tips at $d_e + d_i$ ~2.7 Å in the acceptor region of the plot whereas it is merged within the tip of previously mentioned contact in the donor region. However, the respective plot for an overall structure is symmetric owing to the merging of the asymmetric distribution of points. The significant and quite similar contributions from Cl···H/H···Cl contacts to the Hirshfeld surfaces of *A*, *B* and overall (I), Fig. 9(*d*), have very little influence on the molecular packing due to their interatomic distances being equal to or greater than the sum of their van der Waals radii.

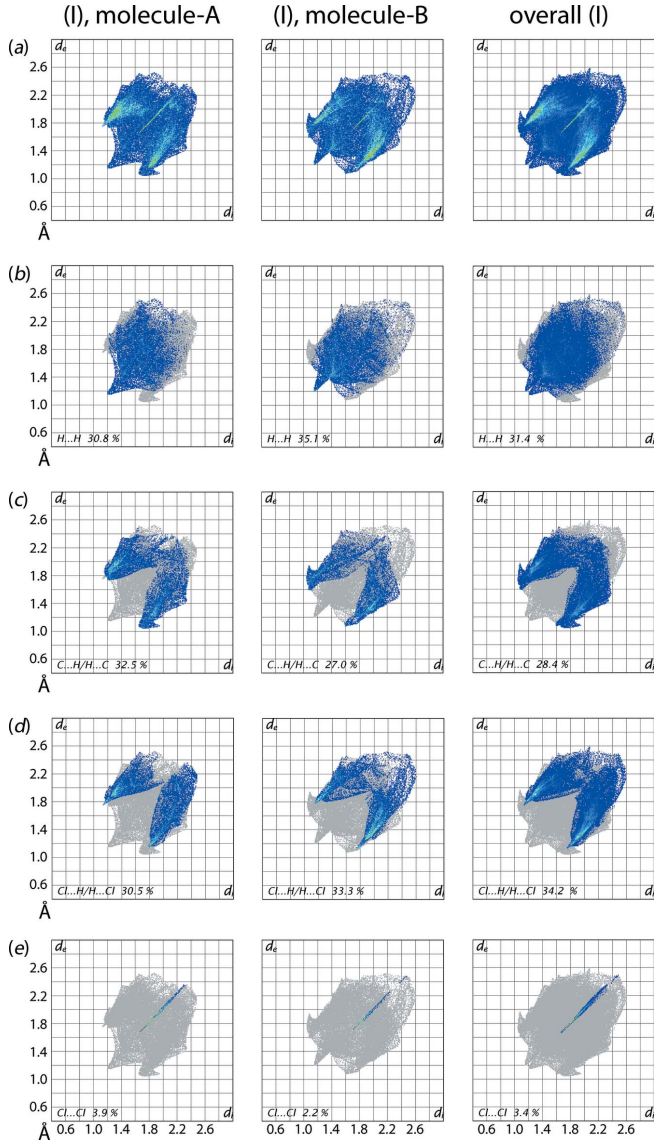

Figure 9
(*a*) The full two-dimensional fingerprint plot for molecule *A* of (I), molecule *B* of (I), and overall (I), and (*b*)–(*e*) those delineated into H···H, C···H/H···C, Cl···H/H···Cl and Cl···Cl contacts.

The linear distribution of points beginning from $d_e + d_i$ ~3.3 and 3.4 Å, Fig. 9(*e*), in the Cl···Cl delineated plots for *A* and *B*, respectively, indicate the presence of Cl···Cl interactions. The small contribution from C···C contacts to the Hirshfeld surface of (I) has a negligible effect on the packing.

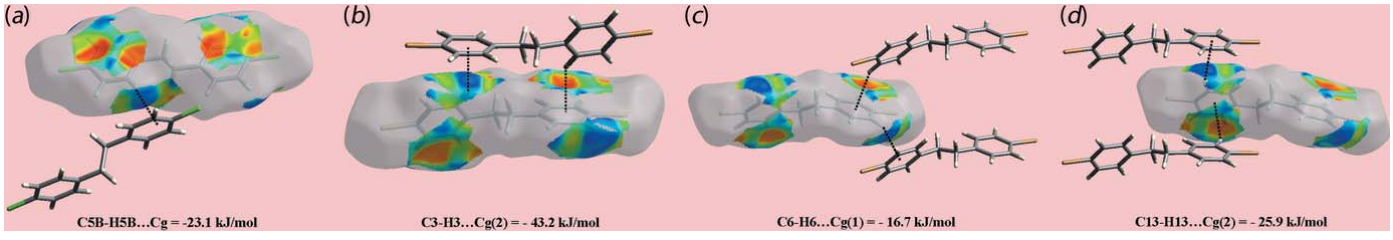

Figure 8
Views of the Hirshfeld surfaces mapped with the shape index property for (*a*) (I), molecule *B*, (*b*)–(*d*) (II), highlighting intermolecular C—H···π interactions through black dotted lines.

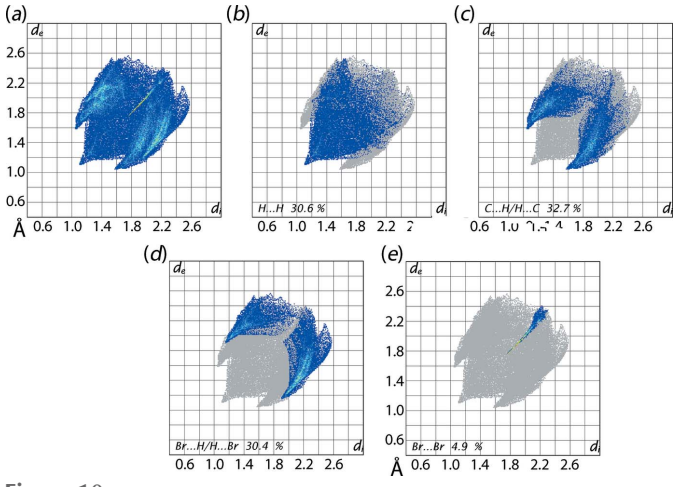

Figure 10
(*a*) The full two-dimensional fingerprint plot for (II), and (*b*)–(*e*) those delineated into H···H, C···H/H···C, Br···Br and Br···H/H···Br contacts.

Comparable fingerprint plots for (II) are shown in Fig. 10 and percentage contributions are collected in Table 4. The short interatomic H···H contact between symmetry-related ethylene-H8*B* atoms is viewed as a single peak at $d_e + d_i$ ~2.2 Å in Fig. 10(*b*). In Fig. 10(*c*), delineated into C···H/H···C contacts, Table 3, the forceps-like tips at $d_e + d_i$ ~2.6 Å reflect the significant C—H···π contacts in the molecular packing. The contribution of Br···H/H···Br contacts to the Hirshfeld surface of (II), Fig. 10(*d*), have very little influence on the packing due to their interatomic distances being around the sum of their van der Waals radii. The short interatomic Br···Br contacts in (II) are viewed as a thin, linear distribution of points initiating from $d_e + d_i$ ~3.5 Å, Fig. 10(*e*). As for (I), the small contribution from C···C contacts to the Hirshfeld surface of (II) has a negligible effect in the crystal.

Table 5
Summary of interaction energies (kJ mol^{-1}) calculated for (I) and (II).

Contact	E_{ele}	E_{pol}	E_{dis}	E_{rep}	E_{tot}
(I)					
Cl1*A*···Cl1*A*	−0.9	0.0	−3.3	7.6	0.9
Cl1*B*···Cl1*B*	−0.9	−0.1	−3.4	5.8	−0.4
C5—H5···*Cg*(C1*A*–C6*A*)	−8.5	−1.5	−33.5	26.1	−23.1
C5···H2*B*	−3.7	−0.8	−18.2	12.9	−12.3
(II)					
Br1···Br2	−2.2	−0.1	−4.9	8.4	0.1
C3—H3···*Cg*(C9–C14)	−14.6	−4.7	−62.4	38.3	−43.2
C6—H6···*Cg*(C1–C6)	−5.6	−1.5	−25.1	15.5	−16.7
C13—H13···*Cg*(C9–C14)	−8.9	−1.9	−30.9	14.2	−25.9
H11···C6	−5.0	−3.2	−50.6	24.7	−32.7
H8*B*···H8*B*	−5.0	−3.2	−50.6	24.7	−32.7

5. Computational chemistry

The pairwise interaction energies between the molecules in the crystals of (I) and (II) were calculated by summing up four energy components, being electrostatic (E_{ele}), polarization

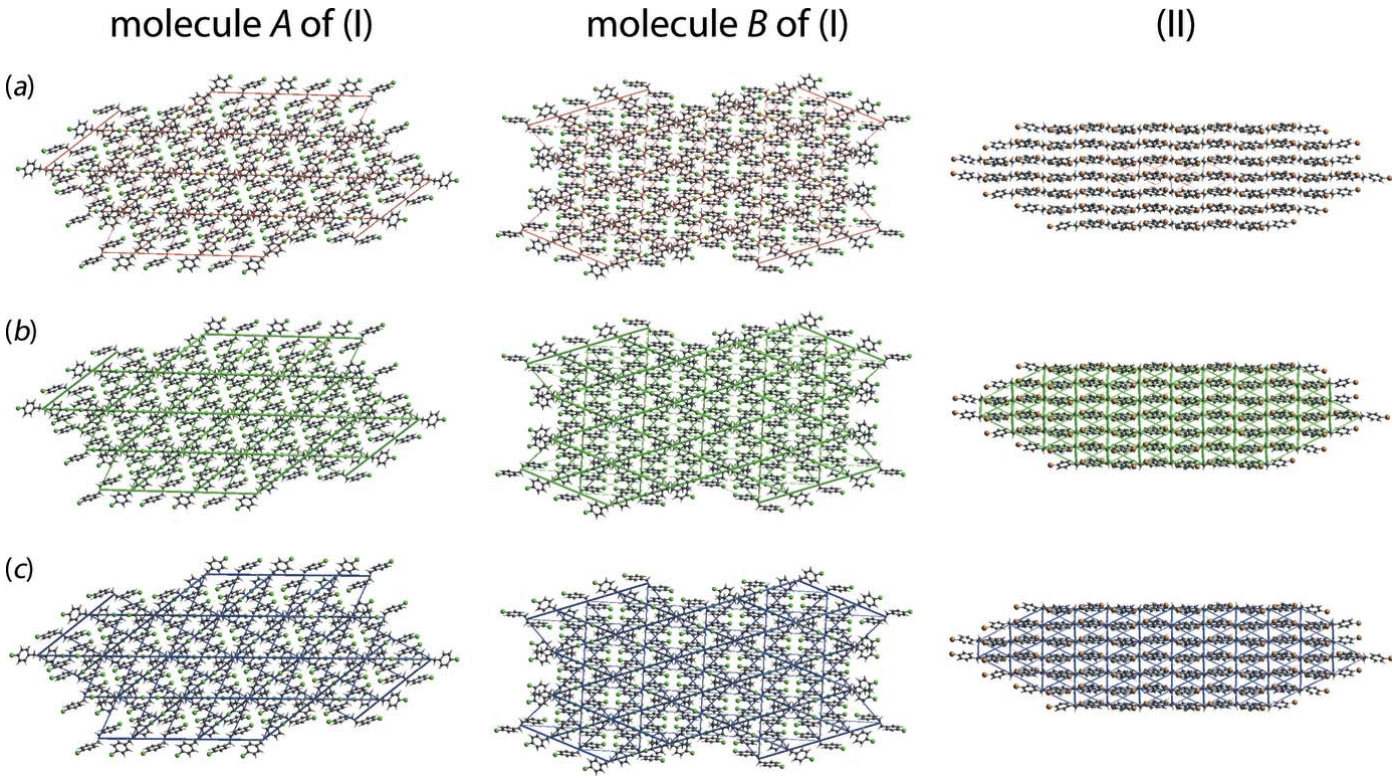

Figure 11
A comparison of the energy frameworks composed of (*a*) electrostatic potential force, (*b*) dispersion force and (*c*) total energy for cluster about a reference molecule of *A* and *B* of (I), and for (II). The energy frameworks were adjusted to the same scale factor of 80 with a cut-off value of 2 kJ mol^{-1} within 4 × 4 × 4 unit cells.

Table 6
Geometric data (Å, °) for halo-substituted 1,2-bis(phenyl)ethane structures.

Ring 1	Ring 2	Symmetry	CH_2-CH_2	dihedral angle C_6/C_6	Reference
2-BrC_6H_4	2-BrC_6H_4	$\bar{1}$	1.540 (7)	0	Kahr *et al.* (1995)
C_6F_5	C_6F_5	$\bar{1}$	1.542 (3)	0	Krafczyk *et al.* (1997)
C_6Br_5	C_6Br_5	$\bar{1}$	1.495 (13)	0	Köppen *et al.* (2007)
4-Br,2,6-$F_2C_6H_2$	4-BrC_6H_4	–	1.522 (10)	1.67 (16)	Galán *et al.* (2016)
4-ClC_6H_4[a]	4-ClC_6H_4	$\bar{1}$	1.530 (2)	0	This work
		$\bar{1}$	1.530 (3)	0	
4-BrC_6H_4	4-BrC_6H_4	–	1.516 (3)	59.29 (11)	This work

Notes: (*a*) Two independent molecules comprise the asymmetric unit.

(E_{pol}), dispersion (E_{dis}) and exchange-repulsion (E_{rep}) (Turner *et al.*, 2017). These energies were obtained by using the wave functions calculated at the B3LYP/6-31G(d,p) level theory for (I) and the HF/STO-3G level theory for (II). The individual energy components as well as total interaction energy relative to reference molecule within molecular clusters out to 3.8 Å. The nature and strength of the energies for the key identified intermolecular interactions are quantitatively summarized in Table 5. Dispersive components are dominant as conventional hydrogen bonding is not possible.

The significant contributions from the C—H$\cdots\pi$ interaction and short interatomic C$\cdots$H/H$\cdots$C contacts in the crystal of (I) are evident from Table 5. Also notable, are the negligible energies associated with the Cl$\cdots$Cl contacts due to the dominance of repulsive contributions. With respect to (II), it is evident from the comparison of the dispersive component as well as total energies for the different interactions that the strength of interactions in the crystal depend upon distance between the respective molecules. The short Br$\cdots$Br contacts in (II) also have very small interaction energies.

The magnitudes of intermolecular energies are represented graphically in the energy frameworks of Fig. 11. Here, the supramolecular architecture of each crystal is viewed through the cylinders joining the centroids of molecular pairs. The red (E_{ele}), green (E_{disp}) and blue (E_{tot}) colour scheme represent the specified energy components. The radii of the cylinders are proportional to the magnitude of interaction energies which are adjusted with a cut-off value of 2 kJ mol^{-1} within 4 × 4 × 4 unit cells. The energy frameworks constructed for the clusters about the independent molecules *A* and *B* of (I) as well as that for (II) also indicate the distinct mode of supramolecular association around the molecules in the molecular packing. The small effect of the electrostatic components and the significant influence of the dispersive components are clearly evident from the energy frameworks shown in Fig. 11.

6. Database survey

There are only four halo-substituted 1,2-bis(phenyl)ethylene derivatives in the literature. The key structural parameters for these are summarized in Table 6. Only one literature structure is not disposed about a centre of inversion, namely the non-symmetric, mixed-halo structure (4-Br,2,6-$F_2C_6H_2$)-$CH_2CH_2C_6H_4$Br-4 (Galán *et al.*, 2016). Generally, the central C_e-C_e (e = ethylene) bonds are long in these compounds with the exception being the pentabromo derivative, $C_6Br_5CH_2CH_2C_6Br_5$ (Köppen *et al.*, 2007).

7. Synthesis and crystallization

Tri(4-chlorobenzyl)tin chloride was prepared by direct synthesis using tin powder (Merck) and 4-chlorobenzyl chloride (Sigma–Aldrich) in water (Sisido *et al.*, 1961). Tri(4-chlorobenzyl)tin chloride (5.3 g, 10 mmol) was dissolved in 95% ethanol (150 ml) and to this was added dropwise 10% sodium hydroxide solution (4 ml). The resulting solution was heated for 1 h. After cooling, the white tri(4-chlorobenzyl)tin hydroxide was filtered off and the filtrate was evaporated slowly to obtain a colourless crystalline solid which was identified crystallographically as (I). Yield: 0.28 g (0.11%). The bromo analogue was similarly obtained as a side-product from the base hydrolysis of tri(4-bromobenzyl)tin bromide. Tri(4-bromobenzyltin) bromide was prepared from the reaction of tin powder (Sigma–Aldrich) and 4-bromobenzyl bromide (Merck) in water (Sisido *et al.*, 1961). Tri(4-bromobenzyl)tin bromide (7.0 g, 10 mmol) was dissolved in 95% ethanol (150 ml) and to this was added 10% sodium hydroxide solution (4 ml). The resulting precipitation was heated for 1 h. After cooling, the yellow tri(4-bromobenzyl)tin hydroxide was filtered off and the filtrate was evaporated slowly to obtain a yellow crystalline solid which was identified crystallographically as (II). Yield: 0.25 g (0.07%)

8. Refinement

Crystal data, data collection and structure refinement details are summarized in Table 7. The carbon-bound H atoms were placed in calculated positions (C—H = 0.93–0.99 Å) and were included in the refinement in the riding-model approximation, with U_{iso}(H) set to 1.2U_{eq}(C). In the refinement of (II), owing to poor agreement the (111) reflection was omitted from the final cycles of refinement.

Acknowledgements

Sunway University Sdn Bhd is thanked for support.

Table 7
Experimental details.

	(I)	(II)
Crystal data		
Chemical formula	$C_{14}H_{12}Cl_2$	$C_{14}H_{12}Br_2$
M_r	251.14	340.06
Crystal system, space group	Monoclinic, *C*2/*c*	Monoclinic, $P2_1/c$
Temperature (K)	296	100
a, *b*, *c* (Å)	26.6755 (19), 9.3259 (7), 10.0405 (8)	10.8761 (2), 7.5157 (1), 15.6131 (3)
β (°)	99.560 (4)	106.177 (1)
V (Å^3)	2463.1 (3)	1225.71 (4)
Z	8	4
Radiation type	Mo $K\alpha$	Mo $K\alpha$
μ (mm^{-1})	0.50	6.58
Crystal size (mm)	0.30 × 0.20 × 0.10	0.20 × 0.11 × 0.07
Data collection		
Diffractometer	Bruker SMART APEX CCD area detector	Bruker SMART APEX CCD area detector
Absorption correction	Multi-scan (*SADABS*; Sheldrick, 1996)	Multi-scan (*SADABS*; Sheldrick, 1996)
T_{min}, T_{max}	0.623, 0.746	0.546, 0.746
No. of measured, independent and observed [$I > 2\sigma(I)$] reflections	12061, 3090, 2627	11908, 3065, 2520
R_{int}	0.026	0.035
(sin $\theta/\lambda)_{max}$ (Å^{-1})	0.669	0.669
Refinement		
$R[F^2 > 2\sigma(F^2)]$, $wR(F^2)$, S	0.033, 0.090, 1.04	0.026, 0.058, 1.03
No. of reflections	3090	3065
No. of parameters	145	145
H-atom treatment	H-atom parameters constrained	H-atom parameters constrained
$\Delta\rho_{max}$, $\Delta\rho_{min}$ (e Å^{-3})	0.31, −0.27	0.45, −0.41

Computer programs: *APEX2* (Bruker, 2008), *SAINT* (Bruker, 2008), *SHELXS97* (Sheldrick, 2008), *SHELXL2018/3* (Sheldrick, 2015), *ORTEP-3 for Windows* (Farrugia, 2012), *DIAMOND* (Brandenburg, 2006), *QMol* (Gans & Shalloway, 2001) and *publCIF* (Westrip, 2010).

References

Bestiuc, I., Buruiana, T., Idriceanu, S., Popescu, V. & Caraculacu, A. (1985). *Rev. Chim.* **36**, 621–623.

Brandenburg, K. (2006). *DIAMOND*. Crystal Impact GbR, Bonn, Germany.

Bruker (2008). *APEX2* and *SAINT*. Bruker AXS Inc., Madison, Wisconsin, USA.

Farrugia, L. J. (2012). *J. Appl. Cryst.* **45**, 849–854.

Galán, E., Perrin, M. L., Lutz, M., van der Zant, H. S. J., Grozema, F. C. & Eelkema, R. (2016). *Org. Biomol. Chem.* **14**, 2439–2443.

Gans, J. & Shalloway, D. (2001). *J. Mol. Graphics Modell.* **19**, 557–559.

Golden, J. H. (1961). *J. Chem. Soc.* pp. 1604–1610.

Hu, Y.-L., Li, F., Gu, G.-L. & Lu, M. (2011). *Catal. Lett.* **141**, 467–473.

Kahr, B., Mitchell, C. A., Chance, J. M., Clark, R. V., Gantzel, P., Baldridge, K. K. & Siegel, J. S. (1995). *J. Am. Chem. Soc.* **117**, 4479–4482.

Köppen, R., Emmerling, F. & Becker, R. (2007). *Acta Cryst.* E**63**, o585–o586.

Krafczyk, R., Thönnessen, H., Jones, P. G. & Schmutzler, R. (1997). *J. Fluor. Chem.* **83**, 159–166.

Liu, J. & Li, B. (2007). *Synth. Commun.* **37**, 3273–3278.

Otsubo, T., Ogura, F., Yamaguchi, H., Higuchi, H. & Misumi, S. (1980). *Synth. Commun.* **10**, 595–601.

Parnes, Z. N., Romanova, V. S. & Vol'pin, M. E. (1989). *Zh. Org. Khim.* **25**, 1075–1079.

Remizov, A. B., Kamalova, D. I. & Stolov, A. A. (2005). *Russ. J. Phys. Chem. A*, **79**(Suppl. 1), 76–80.

Sheldrick, G. M. (1996). *SADABS*. University of Göttingen, Germany.

Sheldrick, G. M. (2008). *Acta Cryst.* A**64**, 112–122.

Sheldrick, G. M. (2015). *Acta Cryst.* C**71**, 3–8.

Sisido, K., Takeda, Y. & Kinugawa, Z. (1961). *J. Am. Chem. Soc.* **83**, 538–541.

Tan, S. L., Jotani, M. M. & Tiekink, E. R. T. (2019). *Acta Cryst.* E**75**, 308–318.

Turner, M. J., Mckinnon, J. J., Wolff, S. K., Grimwood, D. J., Spackman, P. R., Jayatilaka, D. & Spackman, M. A. (2017). *Crystal Explorer 17*. The University of Western Australia.

Westrip, S. P. (2010). *J. Appl. Cryst.* **43**, 920–925.

supporting information

Acta Cryst. (2019). E**75**, 624-631 [https://doi.org/10.1107/S2056989019004742]

1-Chloro-4-[2-(4-chlorophenyl)ethyl]benzene and its bromo analogue: crystal structure, Hirshfeld surface analysis and computational chemistry

Mukesh M. Jotani, See Mun Lee, Kong Mun Lo and Edward R. T. Tiekink

Computing details

For both structures, data collection: *APEX2* (Bruker, 2008); cell refinement: *SAINT* (Bruker, 2008); data reduction: *SAINT* (Bruker, 2008); program(s) used to solve structure: *SHELXS97* (Sheldrick, 2008); program(s) used to refine structure: *SHELXL2018/3* (Sheldrick, 2015); molecular graphics: *ORTEP-3 for Windows* (Farrugia, 2012), *DIAMOND* (Brandenburg, 2006) and *QMol* (Gans & Shalloway, 2001); software used to prepare material for publication: *publCIF* (Westrip, 2010).

1-Chloro-4-[2-(4-chlorophenyl)ethyl]benzene (I)

Crystal data

$C_{14}H_{12}Cl_2$
$M_r = 251.14$
Monoclinic, $C2/c$
$a = 26.6755$ (19) Å
$b = 9.3259$ (7) Å
$c = 10.0405$ (8) Å
$\beta = 99.560$ (4)°
$V = 2463.1$ (3) Å^3
$Z = 8$
$F(000) = 1040$
$D_x = 1.354$ Mg m^{-3}
Mo $K\alpha$ radiation, $\lambda = 0.71073$ Å
Cell parameters from 4470 reflections
$\theta = 3.1$–$28.3°$
$\mu = 0.50$ mm^{-1}
$T = 296$ K
Prism, colourless
0.30 × 0.20 × 0.10 mm

Data collection

Bruker **model?** CCD area detector diffractometer
Radiation source: fine-focus sealed tube
Graphite monochromator
φ and ω scans
Absorption correction: multi-scan (SADABS; Sheldrick, 1996)
$T_{min} = 0.623$, $T_{max} = 0.746$
12061 measured reflections
3090 independent reflections
2627 reflections with $I > 2\sigma(I)$
$R_{int} = 0.026$
$\theta_{max} = 28.4°$, $\theta_{min} = 1.6°$
$h = -35\rightarrow34$
$k = -11\rightarrow12$
$l = -13\rightarrow13$

Refinement

Refinement on F^2
Least-squares matrix: full
$R[F^2 > 2\sigma(F^2)] = 0.033$
$wR(F^2) = 0.090$
$S = 1.04$
3090 reflections
145 parameters
0 restraints
Primary atom site location: structure-invariant direct methods
Hydrogen site location: inferred from neighbouring sites
H-atom parameters constrained
$w = 1/[\sigma^2(F_o^2) + (0.046P)^2 + 1.4907P]$ where $P = (F_o^2 + 2F_c^2)/3$
$(\Delta/\sigma)_{max} = 0.001$

$\Delta\rho_{max}$ = 0.31 e Å^{-3} $\Delta\rho_{min}$ = −0.27 e Å^{-3}

Special details

Geometry. All esds (except the esd in the dihedral angle between two l.s. planes) are estimated using the full covariance matrix. The cell esds are taken into account individually in the estimation of esds in distances, angles and torsion angles; correlations between esds in cell parameters are only used when they are defined by crystal symmetry. An approximate (isotropic) treatment of cell esds is used for estimating esds involving l.s. planes.

Fractional atomic coordinates and isotropic or equivalent isotropic displacement parameters (Å²)

	x	*y*	*z*	U_{iso}*/U_{eq}
Cl1A	0.30558 (2)	0.69571 (4)	0.08421 (3)	0.02990 (11)
C1A	0.35616 (5)	0.64904 (15)	0.20984 (13)	0.0213 (3)
C2A	0.39856 (5)	0.73741 (15)	0.23346 (13)	0.0227 (3)
H2A	0.400392	0.819329	0.181667	0.027*
C3A	0.43825 (5)	0.70121 (14)	0.33594 (13)	0.0224 (3)
H3A	0.466935	0.759394	0.351988	0.027*
C4A	0.43591 (5)	0.57952 (14)	0.41510 (13)	0.0202 (3)
C5A	0.39306 (5)	0.49193 (14)	0.38683 (13)	0.0224 (3)
H5A	0.391223	0.409246	0.437578	0.027*
C6A	0.35314 (5)	0.52569 (15)	0.28454 (13)	0.0237 (3)
H6A	0.324808	0.466334	0.266505	0.028*
C7A	0.47884 (5)	0.54105 (15)	0.52636 (13)	0.0236 (3)
H7A1	0.465754	0.482765	0.592893	0.028*
H7A2	0.492801	0.628077	0.570743	0.028*
Cl1B	0.44971 (2)	0.90465 (4)	0.91449 (4)	0.03360 (12)
C1B	0.39561 (5)	0.87925 (14)	0.79317 (14)	0.0229 (3)
C2B	0.34836 (6)	0.90808 (15)	0.82606 (14)	0.0271 (3)
H2B	0.345284	0.938736	0.912478	0.033*
C3B	0.30571 (5)	0.89060 (15)	0.72836 (15)	0.0274 (3)
H3B	0.273843	0.910620	0.749858	0.033*
C4B	0.30929 (5)	0.84387 (14)	0.59888 (13)	0.0223 (3)
C5B	0.35742 (5)	0.81356 (15)	0.56992 (14)	0.0254 (3)
H5B	0.360595	0.780451	0.484341	0.031*
C6B	0.40064 (5)	0.83161 (15)	0.66564 (14)	0.0258 (3)
H6B	0.432599	0.811998	0.644554	0.031*
C7B	0.26239 (5)	0.82320 (15)	0.49401 (15)	0.0272 (3)
H7B1	0.271471	0.832325	0.404772	0.033*
H7B2	0.238029	0.898025	0.504017	0.033*

Atomic displacement parameters (Å²)

	U^{11}	U^{22}	U^{33}	U^{12}	U^{13}	U^{23}
Cl1A	0.02150 (17)	0.0400 (2)	0.02582 (18)	0.00466 (13)	−0.00301 (12)	0.00464 (14)
C1A	0.0173 (6)	0.0266 (7)	0.0191 (6)	0.0037 (5)	0.0005 (5)	−0.0009 (5)
C2A	0.0226 (6)	0.0237 (6)	0.0222 (6)	0.0005 (5)	0.0051 (5)	0.0011 (5)
C3A	0.0186 (6)	0.0257 (6)	0.0230 (6)	−0.0014 (5)	0.0041 (5)	−0.0029 (5)
C4A	0.0175 (6)	0.0246 (6)	0.0186 (6)	0.0046 (5)	0.0031 (5)	−0.0031 (5)
C5A	0.0230 (6)	0.0206 (6)	0.0236 (6)	0.0016 (5)	0.0035 (5)	0.0009 (5)

C6A	0.0199 (6)	0.0247 (7)	0.0258 (7)	−0.0028 (5)	0.0017 (5)	−0.0024 (5)
C7A	0.0199 (6)	0.0292 (7)	0.0207 (6)	0.0045 (5)	0.0003 (5)	−0.0019 (5)
Cl1B	0.02872 (19)	0.0322 (2)	0.0356 (2)	−0.00182 (13)	−0.00707 (15)	−0.00290 (14)
C1B	0.0223 (6)	0.0199 (6)	0.0251 (6)	−0.0016 (5)	0.0001 (5)	0.0008 (5)
C2B	0.0296 (7)	0.0296 (7)	0.0233 (7)	−0.0023 (5)	0.0076 (6)	−0.0057 (5)
C3B	0.0214 (6)	0.0308 (7)	0.0313 (7)	−0.0006 (5)	0.0084 (5)	−0.0031 (6)
C4B	0.0211 (6)	0.0203 (6)	0.0250 (6)	−0.0005 (5)	0.0024 (5)	0.0028 (5)
C5B	0.0279 (7)	0.0278 (7)	0.0215 (6)	0.0031 (5)	0.0067 (5)	−0.0011 (5)
C6B	0.0216 (6)	0.0280 (7)	0.0286 (7)	0.0041 (5)	0.0069 (5)	0.0002 (5)
C7B	0.0251 (7)	0.0269 (7)	0.0276 (7)	−0.0002 (5)	−0.0011 (6)	0.0033 (6)

Geometric parameters (Å, º)

Cl1A—C1A	1.7424 (13)	Cl1B—C1B	1.7432 (13)
C1A—C6A	1.3829 (19)	C1B—C2B	1.381 (2)
C1A—C2A	1.3877 (18)	C1B—C6B	1.383 (2)
C2A—C3A	1.3899 (18)	C2B—C3B	1.383 (2)
C2A—H2A	0.9300	C2B—H2B	0.9300
C3A—C4A	1.3928 (19)	C3B—C4B	1.3895 (19)
C3A—H3A	0.9300	C3B—H3B	0.9300
C4A—C5A	1.3952 (18)	C4B—C5B	1.3917 (18)
C4A—C7A	1.5043 (17)	C4B—C7B	1.5079 (18)
C5A—C6A	1.3873 (18)	C5B—C6B	1.3832 (19)
C5A—H5A	0.9300	C5B—H5B	0.9300
C6A—H6A	0.9300	C6B—H6B	0.9300
C7A—C7A^{i}	1.530 (2)	C7B—C7B^{ii}	1.530 (3)
C7A—H7A1	0.9700	C7B—H7B1	0.9700
C7A—H7A2	0.9700	C7B—H7B2	0.9700
C6A—C1A—C2A	121.37 (12)	C2B—C1B—C6B	121.11 (12)
C6A—C1A—Cl1A	119.51 (10)	C2B—C1B—Cl1B	119.26 (11)
C2A—C1A—Cl1A	119.12 (10)	C6B—C1B—Cl1B	119.63 (10)
C1A—C2A—C3A	118.77 (12)	C3B—C2B—C1B	118.90 (13)
C1A—C2A—H2A	120.6	C3B—C2B—H2B	120.6
C3A—C2A—H2A	120.6	C1B—C2B—H2B	120.6
C2A—C3A—C4A	121.30 (12)	C2B—C3B—C4B	121.62 (13)
C2A—C3A—H3A	119.4	C2B—C3B—H3B	119.2
C4A—C3A—H3A	119.4	C4B—C3B—H3B	119.2
C3A—C4A—C5A	118.28 (12)	C3B—C4B—C5B	117.94 (12)
C3A—C4A—C7A	121.15 (12)	C3B—C4B—C7B	121.02 (12)
C5A—C4A—C7A	120.55 (12)	C5B—C4B—C7B	121.03 (12)
C6A—C5A—C4A	121.33 (12)	C6B—C5B—C4B	121.43 (13)
C6A—C5A—H5A	119.3	C6B—C5B—H5B	119.3
C4A—C5A—H5A	119.3	C4B—C5B—H5B	119.3
C5A—C6A—C1A	118.92 (12)	C5B—C6B—C1B	118.99 (12)
C5A—C6A—H6A	120.5	C5B—C6B—H6B	120.5
C1A—C6A—H6A	120.5	C1B—C6B—H6B	120.5
C4A—C7A—C7A^{i}	112.14 (13)	C4B—C7B—C7B^{ii}	112.23 (14)

C4A—C7A—H7A1	109.2	C4B—C7B—H7B1	109.2
C7A^{i}—C7A—H7A1	109.2	C7B^{ii}—C7B—H7B1	109.2
C4A—C7A—H7A2	109.2	C4B—C7B—H7B2	109.2
C7A^{i}—C7A—H7A2	109.2	C7B^{ii}—C7B—H7B2	109.2
H7A1—C7A—H7A2	107.9	H7B1—C7B—H7B2	107.9
C6A—C1A—C2A—C3A	−0.98 (19)	C6B—C1B—C2B—C3B	−1.0 (2)
Cl1A—C1A—C2A—C3A	178.52 (10)	Cl1B—C1B—C2B—C3B	178.62 (11)
C1A—C2A—C3A—C4A	−0.5 (2)	C1B—C2B—C3B—C4B	0.5 (2)
C2A—C3A—C4A—C5A	1.63 (19)	C2B—C3B—C4B—C5B	0.5 (2)
C2A—C3A—C4A—C7A	−179.71 (12)	C2B—C3B—C4B—C7B	179.08 (13)
C3A—C4A—C5A—C6A	−1.28 (19)	C3B—C4B—C5B—C6B	−1.2 (2)
C7A—C4A—C5A—C6A	−179.95 (12)	C7B—C4B—C5B—C6B	−179.72 (13)
C4A—C5A—C6A—C1A	−0.2 (2)	C4B—C5B—C6B—C1B	0.8 (2)
C2A—C1A—C6A—C5A	1.3 (2)	C2B—C1B—C6B—C5B	0.3 (2)
Cl1A—C1A—C6A—C5A	−178.18 (10)	Cl1B—C1B—C6B—C5B	−179.24 (11)
C3A—C4A—C7A—C7A^{i}	−83.46 (19)	C3B—C4B—C7B—C7B^{ii}	−83.7 (2)
C5A—C4A—C7A—C7A^{i}	95.17 (17)	C5B—C4B—C7B—C7B^{ii}	94.75 (19)

Symmetry codes: (i) −*x*+1, −*y*+1, −*z*+1; (ii) −*x*+1/2, −*y*+3/2, −*z*+1.

Hydrogen-bond geometry (Å, º)

*Cg*1 is the centroid of the (C1*A*–C6*A*) ring.

D—H···*A*	*D*—H	H···*A*	*D*···*A*	*D*—H···*A*
C5*B*—H5*B*···*Cg*1	0.93	2.62	3.4866 (15)	155

1-Bromo-4-[2-(4-chlorophenyl)ethyl]benzene (II)

Crystal data

$C_{14}H_{12}Br_2$
M_r = 340.06
Monoclinic, $P2_1/c$
a = 10.8761 (2) Å
b = 7.5157 (1) Å
c = 15.6131 (3) Å
β = 106.177 (1)°
V = 1225.71 (4) Å^3
Z = 4
$F(000)$ = 664
D_x = 1.843 Mg m^{-3}
Mo $K\alpha$ radiation, λ = 0.71073 Å
Cell parameters from 3449 reflections
θ = 2.9–28.3°
μ = 6.58 mm^{-1}
T = 100 K
Prism, colourless
0.20 × 0.11 × 0.07 mm

Data collection

Bruker **model?** CCD area detector diffractometer
Radiation source: fine-focus sealed tube
Graphite monochromator
φ and ω scans
Absorption correction: multi-scan (SADABS; Sheldrick, 1996)
T_{min} = 0.546, T_{max} = 0.746
11908 measured reflections
3065 independent reflections
2520 reflections with $I > 2\sigma(I)$
R_{int} = 0.035
θ_{max} = 28.4°, θ_{min} = 2.7°
h = −14→14
k = −10→9
l = −20→20

Refinement

Refinement on F^2
Least-squares matrix: full
$R[F^2 > 2\sigma(F^2)] = 0.026$
$wR(F^2) = 0.058$
$S = 1.03$
3065 reflections
145 parameters
0 restraints

Primary atom site location: structure-invariant direct methods
Hydrogen site location: inferred from neighbouring sites
H-atom parameters constrained
$w = 1/[\sigma^2(F_o^2) + (0.0289P)^2 + 0.0779P]$ where $P = (F_o^2 + 2F_c^2)/3$
$(\Delta/\sigma)_{max} = 0.001$
$\Delta\rho_{max} = 0.45$ e Å^{-3}
$\Delta\rho_{min} = -0.40$ e Å^{-3}

Special details

Geometry. All esds (except the esd in the dihedral angle between two l.s. planes) are estimated using the full covariance matrix. The cell esds are taken into account individually in the estimation of esds in distances, angles and torsion angles; correlations between esds in cell parameters are only used when they are defined by crystal symmetry. An approximate (isotropic) treatment of cell esds is used for estimating esds involving l.s. planes.

Refinement. Owing to poor agreement, the (1 1 1) reflection was omitted from the final cycles of refinement.

Fractional atomic coordinates and isotropic or equivalent isotropic displacement parameters (Å²)

	x	*y*	*z*	U_{iso}*/U_{eq}
Br1	0.50841 (2)	0.84764 (3)	0.90903 (2)	0.02370 (8)
Br2	−0.25048 (2)	0.70383 (3)	0.09773 (2)	0.02253 (8)
C1	0.4150 (2)	0.8055 (3)	0.78827 (15)	0.0159 (5)
C2	0.3013 (2)	0.7135 (3)	0.77050 (15)	0.0161 (4)
H2	0.269796	0.672242	0.817887	0.019*
C3	0.2335 (2)	0.6817 (3)	0.68274 (15)	0.0177 (5)
H3	0.155194	0.617644	0.670292	0.021*
C4	0.2778 (2)	0.7417 (3)	0.61232 (15)	0.0167 (5)
C5	0.3933 (2)	0.8356 (3)	0.63289 (16)	0.0187 (5)
H5	0.425069	0.878319	0.585874	0.022*
C6	0.4624 (2)	0.8674 (3)	0.72041 (15)	0.0173 (5)
H6	0.541066	0.930801	0.733576	0.021*
C7	0.2051 (2)	0.7034 (4)	0.51691 (16)	0.0255 (6)
H7A	0.218424	0.577129	0.503799	0.031*
H7B	0.241041	0.777365	0.477256	0.031*
C8	0.0625 (2)	0.7386 (3)	0.49531 (15)	0.0212 (5)
H8A	0.025232	0.652822	0.529264	0.025*
H8B	0.049949	0.859257	0.516862	0.025*
C9	−0.0116 (2)	0.7260 (3)	0.39829 (14)	0.0147 (4)
C10	−0.1344 (2)	0.7992 (3)	0.36922 (15)	0.0167 (5)
H10	−0.170004	0.854105	0.411688	0.020*
C11	−0.2056 (2)	0.7945 (3)	0.28122 (15)	0.0172 (5)
H11	−0.288380	0.846752	0.263034	0.021*
C12	−0.1540 (2)	0.7119 (3)	0.21965 (15)	0.0161 (4)
C13	−0.0336 (2)	0.6354 (3)	0.24522 (15)	0.0172 (5)
H13	0.000460	0.578442	0.202509	0.021*
C14	0.0369 (2)	0.6430 (3)	0.33433 (15)	0.0154 (4)
H14	0.119669	0.590830	0.352166	0.018*

Atomic displacement parameters (Å²)

	U^{11}	U^{22}	U^{33}	U^{12}	U^{13}	U^{23}
Br1	0.02109 (13)	0.02960 (15)	0.01712 (13)	−0.00317 (9)	−0.00014 (9)	−0.00484 (9)
Br2	0.01971 (13)	0.03068 (15)	0.01471 (12)	−0.00164 (9)	0.00065 (9)	0.00265 (9)
C1	0.0149 (11)	0.0157 (12)	0.0151 (11)	0.0040 (8)	0.0009 (9)	−0.0027 (8)
C2	0.0160 (11)	0.0163 (11)	0.0175 (11)	0.0019 (8)	0.0073 (9)	0.0018 (9)
C3	0.0136 (11)	0.0205 (12)	0.0185 (12)	−0.0004 (8)	0.0036 (9)	−0.0009 (9)
C4	0.0146 (11)	0.0200 (12)	0.0152 (11)	0.0023 (8)	0.0036 (9)	−0.0006 (9)
C5	0.0146 (11)	0.0216 (12)	0.0214 (12)	0.0015 (9)	0.0076 (9)	0.0038 (9)
C6	0.0106 (10)	0.0172 (12)	0.0243 (12)	−0.0004 (8)	0.0053 (9)	−0.0012 (9)
C7	0.0160 (12)	0.0436 (16)	0.0171 (12)	0.0027 (10)	0.0050 (10)	−0.0026 (11)
C8	0.0166 (12)	0.0281 (13)	0.0172 (12)	0.0018 (10)	0.0021 (9)	−0.0023 (10)
C9	0.0169 (11)	0.0132 (11)	0.0146 (11)	−0.0018 (8)	0.0054 (9)	0.0007 (8)
C10	0.0173 (11)	0.0152 (12)	0.0195 (12)	−0.0002 (8)	0.0082 (9)	0.0003 (9)
C11	0.0129 (10)	0.0172 (12)	0.0211 (12)	0.0006 (8)	0.0039 (9)	0.0026 (9)
C12	0.0160 (11)	0.0175 (12)	0.0133 (10)	−0.0038 (8)	0.0015 (9)	0.0025 (9)
C13	0.0189 (11)	0.0165 (12)	0.0174 (11)	−0.0011 (9)	0.0070 (9)	−0.0003 (9)
C14	0.0129 (11)	0.0160 (11)	0.0176 (11)	−0.0012 (8)	0.0048 (9)	0.0015 (9)

Geometric parameters (Å, º)

Br1—C1	1.902 (2)	C7—H7B	0.9900
Br2—C12	1.901 (2)	C8—C9	1.507 (3)
C1—C2	1.376 (3)	C8—H8A	0.9900
C1—C6	1.382 (3)	C8—H8B	0.9900
C2—C3	1.384 (3)	C9—C10	1.399 (3)
C2—H2	0.9500	C9—C14	1.399 (3)
C3—C4	1.393 (3)	C10—C11	1.377 (3)
C3—H3	0.9500	C10—H10	0.9500
C4—C5	1.398 (3)	C11—C12	1.388 (3)
C4—C7	1.507 (3)	C11—H11	0.9500
C5—C6	1.385 (3)	C12—C13	1.384 (3)
C5—H5	0.9500	C13—C14	1.390 (3)
C6—H6	0.9500	C13—H13	0.9500
C7—C8	1.516 (3)	C14—H14	0.9500
C7—H7A	0.9900		
C2—C1—C6	121.4 (2)	C9—C8—C7	116.1 (2)
C2—C1—Br1	119.02 (17)	C9—C8—H8A	108.3
C6—C1—Br1	119.57 (17)	C7—C8—H8A	108.3
C1—C2—C3	119.2 (2)	C9—C8—H8B	108.3
C1—C2—H2	120.4	C7—C8—H8B	108.3
C3—C2—H2	120.4	H8A—C8—H8B	107.4
C2—C3—C4	121.3 (2)	C10—C9—C14	117.4 (2)
C2—C3—H3	119.4	C10—C9—C8	119.73 (19)
C4—C3—H3	119.4	C14—C9—C8	122.9 (2)
C3—C4—C5	117.9 (2)	C11—C10—C9	122.3 (2)

C3—C4—C7	121.1 (2)	C11—C10—H10	118.8
C5—C4—C7	120.9 (2)	C9—C10—H10	118.8
C6—C5—C4	121.3 (2)	C10—C11—C12	118.6 (2)
C6—C5—H5	119.3	C10—C11—H11	120.7
C4—C5—H5	119.3	C12—C11—H11	120.7
C1—C6—C5	118.8 (2)	C13—C12—C11	121.3 (2)
C1—C6—H6	120.6	C13—C12—Br2	119.32 (17)
C5—C6—H6	120.6	C11—C12—Br2	119.41 (17)
C4—C7—C8	114.2 (2)	C12—C13—C14	119.0 (2)
C4—C7—H7A	108.7	C12—C13—H13	120.5
C8—C7—H7A	108.7	C14—C13—H13	120.5
C4—C7—H7B	108.7	C13—C14—C9	121.4 (2)
C8—C7—H7B	108.7	C13—C14—H14	119.3
H7A—C7—H7B	107.6	C9—C14—H14	119.3

C6—C1—C2—C3	0.3 (3)	C7—C8—C9—C10	−163.7 (2)
Br1—C1—C2—C3	−179.64 (16)	C7—C8—C9—C14	16.4 (3)
C1—C2—C3—C4	−0.3 (3)	C14—C9—C10—C11	−1.3 (3)
C2—C3—C4—C5	0.0 (3)	C8—C9—C10—C11	178.8 (2)
C2—C3—C4—C7	178.7 (2)	C9—C10—C11—C12	0.9 (3)
C3—C4—C5—C6	0.4 (3)	C10—C11—C12—C13	0.0 (3)
C7—C4—C5—C6	−178.3 (2)	C10—C11—C12—Br2	−179.99 (16)
C2—C1—C6—C5	0.0 (3)	C11—C12—C13—C14	−0.5 (3)
Br1—C1—C6—C5	179.96 (16)	Br2—C12—C13—C14	179.49 (16)
C4—C5—C6—C1	−0.4 (3)	C12—C13—C14—C9	0.1 (3)
C3—C4—C7—C8	46.6 (3)	C10—C9—C14—C13	0.7 (3)
C5—C4—C7—C8	−134.8 (2)	C8—C9—C14—C13	−179.4 (2)
C4—C7—C8—C9	172.1 (2)		

Hydrogen-bond geometry (Å, º)

*Cg*1 and *Cg*2 are the centroids of the (C1–C6) and (C9–C14) rings, respectively.

D—H···*A*	*D*—H	H···*A*	*D*···*A*	*D*—H···*A*
C3—H3···*Cg*2^{i}	0.95	2.69	3.442 (2)	136
C6—H6···*Cg*1^{ii}	0.95	2.91	3.704 (2)	141
C13—H13···*Cg*2^{iii}	0.95	2.87	3.569 (2)	131

Symmetry codes: (i) −*x*, −*y*+1, −*z*+1; (ii) −*x*+1, *y*+1/2, −*z*+3/2; (iii) −*x*, *y*−1/2, −*z*+1/2.